# Neutral thermospheric dynamics observed with two scanning Doppler imagers: 2. Vertical winds

C. Anderson,[1] M. Conde,[1] and M. G. McHarg[2]

Received 13 September 2011; revised 18 January 2012; accepted 19 January 2012; published 6 March 2012.

[1] This article is the second in a series of three papers reporting on observations of the 630.0 nm thermospheric airglow emission by two spatially separated scanning Doppler imagers (SDI's) in Alaska. In this article, line-of-sight wind measurements from these instruments in four common-volume regions lying along the great circle joining the two observatories have been used to derive estimates of the vertical wind in those common-volumes. These estimates are combined with the vertical winds measured directly in each of the station zeniths to resolve both the spatial and temporal variations of the vertical wind field. Data from four nights are presented as examples of the wave-like oscillations and frequently high spatial correlations that are observed. A statistical study of data from the full 19-night data set showed that the frequency of observing statistically significant correlation between vertical winds measured at separate locations decreased linearly with increasing separation. A linear fit to this trend indicated that for this particular location and orientation the largest separation over which statistically significant correlation would be expected to occur is approximately 540 km.

**Citation:** Anderson, C., M. Conde, and M. G. McHarg (2012), Neutral thermospheric dynamics observed with two scanning Doppler imagers: 2. Vertical winds, *J. Geophys. Res.*, *117*, A03305, doi:10.1029/2011JA017157.

## 1. Introduction

[2] At altitudes above approximately 120 km the combination of a strongly positive temperature gradient and a kinematic viscosity that increases exponentially with altitude acts together to strongly oppose vertical motion of atmospheric gas parcels normal to constant pressure surfaces. However, many studies have reported strong vertical winds of 100 m $s^{-1}$ or more [e.g., *Spencer et al.*, 1982; *Sica et al.*, 1986; *Wardill and Jacka*, 1986; *Smith and Hernandez*, 1995; *Innis et al.*, 1996, 1999; *Innis and Conde*, 2002]. Strong vertical winds can play an important role in upper atmospheric composition, by transporting species to new altitudes at which they may no longer be in chemical equilibrium [*Smith*, 1998]. Vertically transported species may substantially alter the production and loss rates of neutral and/or ionospheric species at their new altitude, and these changes may be transported long distances by horizontal advection.

[3] To date, the majority of vertical wind measurements presented in the literature have come from passive ground-based optical instruments (typically Fabry-Perot interferometers) and instruments on-board satellites (for example Dynamics Explorer 2). Ground-based instruments, when used in isolation, can only resolve vertical winds in the local zenith, however they are well suited to monitoring the temporal evolution of the wind. In contrast, satellites essentially record the spatial variation of the vertical wind field along an orbital track, but are not well suited to monitoring the temporal evolution of that field.

[4] Typically, vertical wind magnitudes are very small, frequently less than 30 m $s^{-1}$ [e.g., *Conde and Dyson*, 1995; *Greet et al.*, 2002]. Measurement of such small-magnitude winds requires high instrumental stability. In the case of optical spectrometers, there are also issues involving the choice of a zero Doppler baseline from which wind speeds are determined [see, e.g., *Aruliah and Rees*, 1995]. For these reasons upper atmospheric vertical winds have not been as extensively studied as, for example, have horizontal winds, and our understanding of the physical mechanisms and scale lengths governing vertical winds is correspondingly less well developed.

[5] At low and mid latitudes, vertical winds are observed to be of small magnitude [e.g., *Hernandez*, 1982; *Biondi*, 1984; *Biondi and Sipler*, 1985; *Sipler et al.*, 1995], and sometimes show periodic oscillations consistent with gravity waves [*Hernandez*, 1982]. At high latitudes, there have been a number of reports of very large magnitude vertical winds [see, e.g., *Smith*, 2000, and references therein], and the observed vertical winds tend to show more variability. Vertical winds inferred from Dynamics Explorer 2 data have reinforced the picture of occasionally large, highly variable vertical winds at high latitudes, and relatively quiescent

[1]Geophysical Institute, University of Alaska Fairbanks, Fairbanks, Alaska, USA.
[2]Physics Department, U.S. Air Force Academy, Colorado Springs, Colorado, USA.

Copyright 2012 by the American Geophysical Union.
0148-0227/12/2011JA017157

vertical winds at low and mid latitudes [*Spencer et al.*, 1982; *Innis and Conde*, 2002]. Furthermore, a number of studies have observed a tentative link between vertical wind direction and the relative location of the aurora at F region heights, with upward/downward vertical winds on the poleward/equatorward edge of the nightside auroral oval [e.g., *Price et al.*, 1995; *Innis et al.*, 1996, 1999; *Ishii et al.*, 2001; *Greet et al.*, 2002; *Ishii*, 2005].

[6] Dual-wavelength optical interferometers have been used to infer vertical winds from optical emissions originating at different altitudes. Typically these instruments have simultaneously observed the 557.7 nm and 630.0 nm emissions of atomic oxygen, originating in the E region ($\sim$120 km) and F-region ($\sim$240 km) thermosphere respectively. *Price et al.* [1995], for example, observed positively correlated upwellings above Poker Flat, Alaska, at these altitudes on two geomagnetically active ($K_p$ = 7) nights. Similar measurements were reported by *Ishii et al.* [2001], also from Poker Flat, where discrete (in time) E- and F-region vertical wind disturbances were often positively correlated. *Ishii et al.* [1999] observed periods of both positive and negative correlation between upper and lower thermospheric vertical winds measured above Ramfjord, in Norway, while *Kosch et al.* [2000] observed positive correlation between vertical winds at these altitudes that increased with increasing geomagnetic activity. E region vertical winds have also been inferred from tristatic radar measurements [e.g., *Oyama et al.*, 2008].

[7] In the studies cited above no significant time-lag was observed between the lower and upper thermospheric vertical wind events. *Deng and Ridley* [2007] used a global circulation model (the Global Ionosphere-Thermosphere Model, or GITM [see *Ridley et al.*, 2006]) to show that while heat deposition due to Joule heating maximizes around 120 km altitude, the neutral gas heating rate (in units of K $s^{-1}$) actually maximizes at much higher altitudes, around 400 km, owing to the exponential decrease of neutral gas density with increasing altitude. These modeling results suggest that the ratio of the neutral gas heating rate at 240 km to that at 120 km should not be much greater than approximately 2:1 [see also *Thayer and Semeter*, 2004]. In cases where discrete vertical wind disturbances are driven by in-situ forces such as localized heating (and are therefore not due to propagating waves) positive correlation between upper and lower thermospheric vertical winds may be expected without any significant time delay.

[8] The typical horizontal scale sizes of individual regions of vertical motion are still not well understood. *Spencer et al.* [1982] reported measurements from the Dynamics Explorer 2 (DE-2) satellite that showed very strong (100–200 m $s^{-1}$) upward vertical winds at altitudes between 300–500 km. The latitudinal extent of these vertical motions was on the order of 400–500 km, and they frequently correlated well with peaks in the zonal wind speed. At an altitude of 240 km, *Crickmore* [1993] estimated a horizontal scale size of approximately 360 km, using single-station Fabry-Perot interferometer data recorded at Halley, Antarctica. This estimate was derived by comparing an observed relationship between vertical wind and horizontal divergence with the theoretical relationship predicted by *Burnside et al.* [1981]. Through a consideration of power and continuity requirements, *Price et al.* [1995] estimated upper bounds on the vertical wind horizontal scale size of 320 km and 800 km, in the lower and upper thermosphere respectively. This estimate also relied on single-station Fabry-Perot interferometer data, recorded at Poker Flat, Alaska.

[9] In contrast, vertical wind studies by *Kosch et al.* [2000] and *Ishii et al.* [2004] have indicated much smaller horizontal scale sizes. In the former study, vertical winds at both lower and upper thermospheric altitudes were measured by two Fabry-Perot interferometers (FPIs) separated by a predominantly longitudinal baseline of only $\sim$45 km [*Kosch et al.*, 2000]. Essentially no correlation was observed between the two locations at either altitude.

[10] *Ishii et al.* [2004] reported similar observations of lower and upper thermospheric vertical winds from two locations in Alaska at similar geomagnetic latitudes but separated by approximately 300 km. These authors observed a high degree of correlation in the lower thermospheric vertical winds measured at each station, however the correlation in the upper thermospheric winds was relatively low. Recent bistatic vertical wind observations between two FPIs in Antarctica have indicated that the horizontal correlation length can vary between $\sim$150-480 km [*Anderson et al.*, 2011].

[11] Horizontal (and vertical) correlation lengths will naturally depend on the underlying driving forces. As mentioned above, for vertical motions driven in-situ by localized heating, horizontal scale lengths would depend on the horizontal extent of the heated region. Small-scale current systems, for example, can be associated with large heat inputs due to the concentration of perturbation Poynting flux [e.g. *Richmond* 2010]. For aurorally driven heating, the heating region should be aligned approximately parallel to the auroral oval, and therefore we would not expect the scale length to be isotropic. Large-scale horizontal divergence could in principle drive similarly large-scale vertical winds [see, e.g., *Guo and McEwen*, 2003]. Gravity waves are another possible source of vertical motions, in which case the correlation lengths will depend on the direction of propagation (the alignment of the perturbation phase-fronts) and wavelength.

[12] Wave-like vertical oscillations have been observed in DE-2 data at latitudes within the nominal auroral oval [*Johnson et al.*, 1995; *Innis and Conde*, 2002]. *Johnson et al.* [1995] concluded that these oscillations were due to gravity waves propagating from the nightside to the dayside. Maps of neutral vertical wind activity (measured by vertical wind variance along the orbital track) produced by *Innis and Conde* [2002] clearly showed the region of elevated vertical wind activity to be bounded by the statistical location of the auroral oval. These results indicate that the likelihood of observing wave-like oscillations in vertical wind measurements should be greater poleward of the auroral oval [see, e.g., *Ishii et al.*, 1999].

[13] Investigations of neutral vertical winds using first principles-based numerical simulations have typically focused on the thermospheric response to Joule and particle heating associated with auroral arcs. *Rees et al.* [1984], for example, used a three-dimensional, hydrostatic, global-scale model (described by *Fuller-Rowell and Rees* [1980]) and reported simulated vertical winds (as would be seen by a ground-based FPI) of $\sim$100 m $s^{-1}$ in response to only 2 min of auroral heating (at 50 mW $m^{-2}$). Higher resolution, non-hydrostatic, two-dimensional models were employed

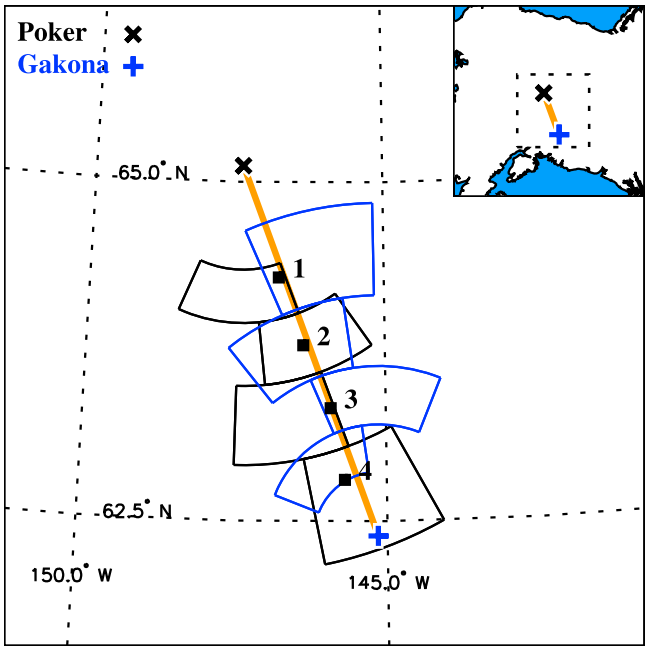


**Figure 1.** Locations of the Poker Flat (black) and Gakona (blue) instruments. Bistatic vertical wind locations are shown as black squares, along with the Poker Flat (black) and Gakona (blue) zones in which bistatic spectra were accumulated. The yellow line indicates the Gakona-Poker Flat great circle.

by *Fuller-Rowell* [1985], *Walterscheid et al.* [1985], *Walterscheid and Lyons* [1992], *Shinagawa et al.* [2003], and *Shinagawa and Oyama* [2006]. These simulations produced vertical winds of typical magnitude 20 m $s^{-1}$ within the auroral arcs, and generated gravity waves that propagated away from the auroral source. *Shinagawa and Oyama* [2006] observed that larger vertical wind oscillations were produced when the background meridional flow was larger than ~300 m $s^{-1}$, and the oscillatory structure was observed downwind of the auroral heating, as suggested by *Smith* [2000].

[14] *Sun et al.* [1995] developed a three-dimensional, non-hydrostatic, high-resolution model to study the thermospheric response to morningside diffuse aurora. These authors performed their simulation separately in two and three dimensions, and observed a much weaker response in the three-dimensional case, highlighting the importance of fully three-dimensional modeling. Vertical wind magnitudes reported by *Sun et al.* [1995] were of the order of meters per second, and both east-west and north-south propagating gravity waves were generated, with faster propagation in the north-south direction.

[15] *Deng et al.* [2008] reported on results obtained with the three-dimensional, non-hydrostatic, Global Ionosphere-Thermosphere Model [*Ridley et al.*, 2006]. *Deng et al.* [2008] were able to generate vertical winds of 150 m $s^{-1}$ at 300 km altitude in response to a sudden intense enhancement of high-latitude Joule heating (driven by a sudden increase in the magnitude of the IMF). The large vertical wind was driven by a propagating acoustic wave. Using the same model, *Yiğit and Ridley* [2011] have shown that increased model spatial resolution leads to increased vertical wind magnitudes due to better electric field resolution and larger relative ion-neutral flows (and therefore enhanced Joule heating), and that sudden changes in ion flow (i.e. step-changes) produce larger vertical winds with larger variance compared with steady ion flows.

[16] Vertical wind maps presented by *Yiğit and Ridley* [2011] showed vertical wind structures at scales down to approximately 30° × 2.5° (longitude × latitude) in their highest resolution simulations (2.5° longitude × 0.3125° latitude), structures that were not captured in lower-resolution model runs. The corresponding distance scales for these structures were on the order of 600 km × 300 km (east-west × north-south).

[17] The picture that has emerged from these studies supports a vertical wind field that is frequently correlated over a vertical scale of order 200 km, and with a horizontal scale size that can be anywhere from less than 50 km up to approximately 800 km, depending on (among other things) the level of geomagnetic activity and orientation relative to auroral heat sources. Vertical winds may be a result of in-situ heating or propagating waves (predominantly gravity waves, with possible contributions from acoustic waves), or advection of vertical momentum.

[18] In the work by *Anderson et al.* [2012, hereinafter Paper 1], horizontal wind measurements were presented from two scanning Doppler imagers operating in Alaska. In particular, bistatic inversion of line-of-sight wind samples at locations common to both instruments were presented. In the current article, the bistatic inversion technique has been used to derive vertical wind measurements in four common volumes located along the great circle between the Gakona and Poker Flat instruments. We have used these measurements in addition to those made in the station zeniths to investigate two key aspects of the vertical wind: 1) the statistical distribution of vertical wind speeds, to better understand both the typical vertical wind magnitudes and the frequency with which large (>50 m $s^{-1}$) vertical winds are observed, and 2) the typical horizontal spatial scales over which correlated vertical wind events are most frequently recorded.

## 2. Instrumentation

[19] The two optical interferometers used in this study have been described in Paper 1. These Doppler imagers combine all-sky fore-optics with separation-scanned Fabry-Perot etalons to record spectra from 115 locations simultaneously across the sky. One of these scanning Doppler imagers (SDIs) is owned by the Geophysical Institute and is located at Poker Flat, Alaska, the other is owned by the United States Air Force Academy, and is located at Gakona, Alaska. The locations of these instruments in relation to the Alaskan coastline is shown in the inset in the top right corner of Figure 1.

## 3. Analysis

[20] The details of the bistatic inversion algorithm used in this study have been described in Paper 1. In summary, line-of-sight wind estimates in common observing volumes between the two SDIs were used to solve uniquely for two of the three components of the neutral wind vector in the common-volume. Specifically the two wind components that are resolved using this technique are those lying in the

plane whose normal is defined by the cross-product of the lines-of-sight from each instrument to the common-volume. The wind components are then calculated relative to coordinate axes contained in this plane (herein referred to as the 'viewing-plane'). These axes are designated $\hat{\mathbf{l}}$ (horizontal and directed parallel to the great circle between the two instruments, with positive in the direction from Gakona to Poker Flat) and $\hat{\mathbf{m}}$ (perpendicular to the great circle, and making an angle $\eta$ with the local zenith).

[21] The absolute orientation of the $\hat{\mathbf{l}}$ axis is constant, however the orientation of the $\hat{\mathbf{m}}$ axis (the angle $\eta$ that it makes with the local zenith) varies with distance away from the Gakona-Poker Flat great circle. Thus, at large distances from the Gakona-Poker Flat great circle, the resolved bistatic wind component parallel to $\hat{\mathbf{m}}$ is dominated by the horizontal wind (in the direction perpendicular to the great circle) while for volumes close to the great circle this wind component is dominated by the vertical wind.

[22] The angle $\eta$ is one parameter used to filter the bistatic wind results. Another is the dot product between the lines-of-sight from each instrument to the common-volume. This parameter is denoted by $\chi$ and quantifies the degree to which the instruments are looking along the same line-of-sight. Values of $\chi$ close to 1 indicate that both instruments are observing substantially along the same line-of-sight, and therefore the bistatic inversion will be ill-determined. In practice restricting $\chi$ to less than 0.82 ensures that at the filtered bistatic locations the inversion is sufficiently robust for the majority of the time.

[23] In the current work bistatic vertical wind locations were chosen as those for which $\eta < 3°$ and $\chi < 0.5$. This restricted the available bistatic locations to the four shown in Figure 1. Common-volume (CV) locations will be referred to by number as indicated in Figure 1. The projection of the SDI viewing zones (onto a fixed altitude of 240 km) from which the bistatic data were acquired are shown as the annular segments in Figure 1, with color indicating to which instrument the zone belongs (black for Poker Flat, blue for Gakona).

## 4. Results

[24] The current data set of bistatic results consists of 19 nights between January 20, 2010 and December 29, 2010, inclusive. These nights were selected for bistatic analysis based on visual inspection of the monostatic wind fields routinely inferred from each instrument, from which it was relatively easy to determine which nights were cloud-free at both locations. The data set was dominated by observations made during quiet geomagnetic conditions, with the aurora to the north of Poker Flat. Four nights will be presented in detail here. These nights demonstrate the often good correlation between vertical winds even across the largest separation of 333 km (the great circle distance between Gakona and Poker Flat), as well as the wave-like features that are sometimes observed.

### 4.1. January 24, 2010

[25] In Paper 1 the horizontal monostatic and bistatic winds inferred on January 24, 2010 were presented. In Figure 2 the station zenith and bistatically derived vertical winds from this same night are presented. The left column of this figure displays the vertical winds (as data points) recorded at each bistatic location in addition to the vertical winds measured above each station. Error-bars indicate the $\pm 1\sigma$ uncertainty in the fitted Doppler velocity estimates, or in the case of the bistatic data the uncertainty in the derived vertical wind based on the uncertainties in the underlying data. For clarity, only every third error-bar is shown for the bistatic data. The solid curve shows the vertical wind data smoothed by a Gaussian window of 4 min half-width. All plots are ordered from top to bottom by increasing distance from Poker Flat, and the y axis is shown on alternating sides of each time series.

[26] Note that, as explained in Paper 1, the bistatic data are derived from a union of the two individual data sets from each instrument, and therefore the time resolution of the bistatic data appears higher than that of either of the two instruments. The apparently higher time resolution is simply a consequence of the bistatic analysis scheme adopted.

[27] The middle column displays the corresponding intensity time series at each location in arbitrary units. At the bistatic locations, the average of both the Gakona and Poker Flat intensity measurements are shown for that location. The right column shows the corresponding temperature time series relative to the nightly mean temperature calculated from the given time series. Temperatures at bistatic locations have been averaged between instruments in the same way as the intensities. Temperature estimates are typically noisier than speed or intensity estimates, and thus the solid curves show 15 minute (Gaussian half-width) smoothed temperatures to aid interpretation.

[28] The grey shaded polygon in each column highlights a time period of interest for this day. During this time period all locations observed a systematic upward acceleration. In all regions except CV 3 this resulted in a change of wind direction from downward to upward, and peak upward wind speeds of 15-25 $ms^{-1}$ were reached. Each location observed this event at different times, as indicated by the slant-angle of the shaded region. It was observed earliest in the Gakona zenith, and latest above Poker Flat, with a time lag of approximately 1 hour.

[29] The time ordering is interesting, as this period corresponded to a magnetic equatorward excursion of the auroral oval (0600–0715 UT) as determined from 630.0 nm all-sky images derived from the SDI data (not shown here). At the peak of the excursion (0715 UT), the oval was approximately overhead of Poker Flat and filled the northern half of the Poker Flat SDI field-of-view. The oval then contracted poleward between 0715 and 0830 UT. Gakona is approximately 2.4° magnetically south of Poker Flat, thus one might expect that Poker Flat would be the first to observe aurorally driven wind events. If the disturbance was caused by propagating waves, then interpretation becomes more difficult. We also note that the vertical wind direction was in qualitative agreement with previous studies that have observed downward winds on the equatorward edge of auroral arcs, and upward winds on the poleward edge [e.g., *Crickmore et al.*, 1991; *Innis et al.*, 1996; *Greet et al.*, 2002; *Ishii*, 2005].

[30] Spatial correlation of vertical winds during the remainder of the night was variable, however the temperature variations (relative to the nightly mean temperature at each location) showed similar time evolution from

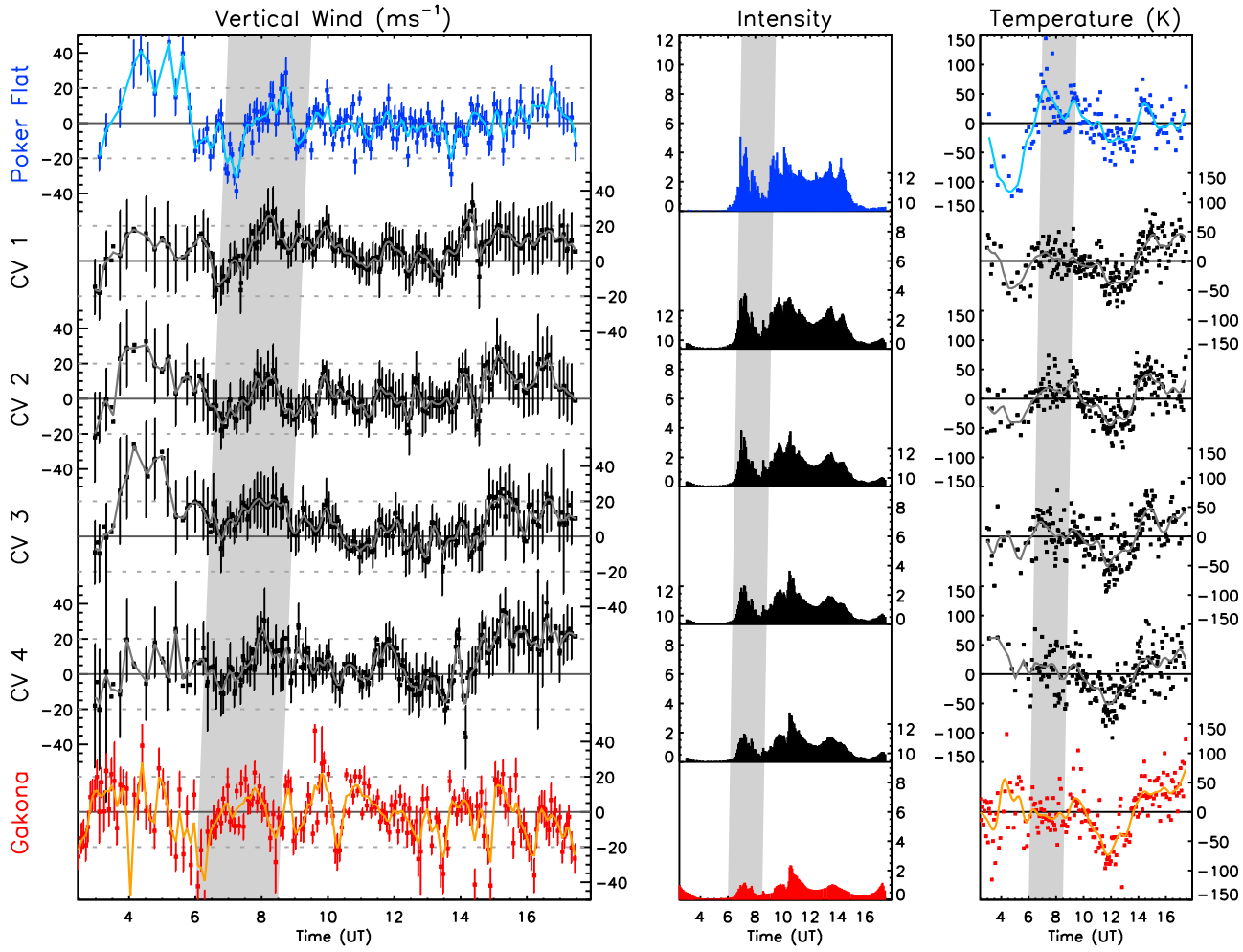


**Figure 2.** (left) Vertical wind, (middle) intensity, and (right) temperature in the station zeniths and at each bistatic location for the night of January 24, 2010. Solid curves in the vertical wind and temperature panels are time-smoothed versions of the data shown by the data points (the smoothing window half-width was 4 min and 15 min respectively for the vertical winds and temperatures). Median temperature uncertainty was 23 K.

approximately 1000 UT onwards. The correlated temperature reduction that peaked at 1200 UT, for example, was not obviously associated with any large-scale vertical winds. This reduction in temperature was followed by a temperature increase above the nightly mean at all locations.

### 4.2. April 5, 2010

[31] Data for the night of April 5, 2010 are shown in Figure 3. This night was geomagnetically very disturbed, with horizontal magnetic field readings at Fort Yukon reaching -2000 nT (see Figure 4). As a result of this activity the auroral oval (as determined from SDI all-sky images) during the time period displayed in Figure 3 was magnetically southward of Gakona, and thus both stations were located within the geomagnetic polar cap. This is highly relevant, since it is within the nominal auroral oval region that wave-like oscillations are most frequently observed [*Innis and Conde*, 2002].

[32] The vertical winds and temperatures observed on this night were at times highly correlated at all sampled scales. The major disturbance began at 0830 UT, with upward winds observed at all locations except above Poker Flat. A strong, 40–50 m s$^{-1}$ downward wind was then observed concurrently at all locations (1000 UT). Following this downward wind, winds at locations northward of and including CV 2 reversed sign to become positive, while at locations southward of and including CV 3 the downward wind reduced in magnitude but did not become positive, and a second strong downward wind was observed near 1045 UT.

[33] At approximately 1130 UT a large (>40 m s$^{-1}$) upward wind was observed above Poker Flat and in CV 1. Upward winds were also observed concurrently in CV's 2, 3 and 4, with magnitudes that decreased with increasing distance from Poker Flat. Above Gakona there was no significant vertical wind at that time. The subsequent downward wind was clearly observed at all locations, however it was not observed concurrently in all locations. Instead, it was observed at progressively later times at higher magnetic latitudes.

[34] Associated with the vertical wind oscillations were temperature fluctuations on the order of 100 K. Vertical winds and temperature fluctuations (relative to the nightly

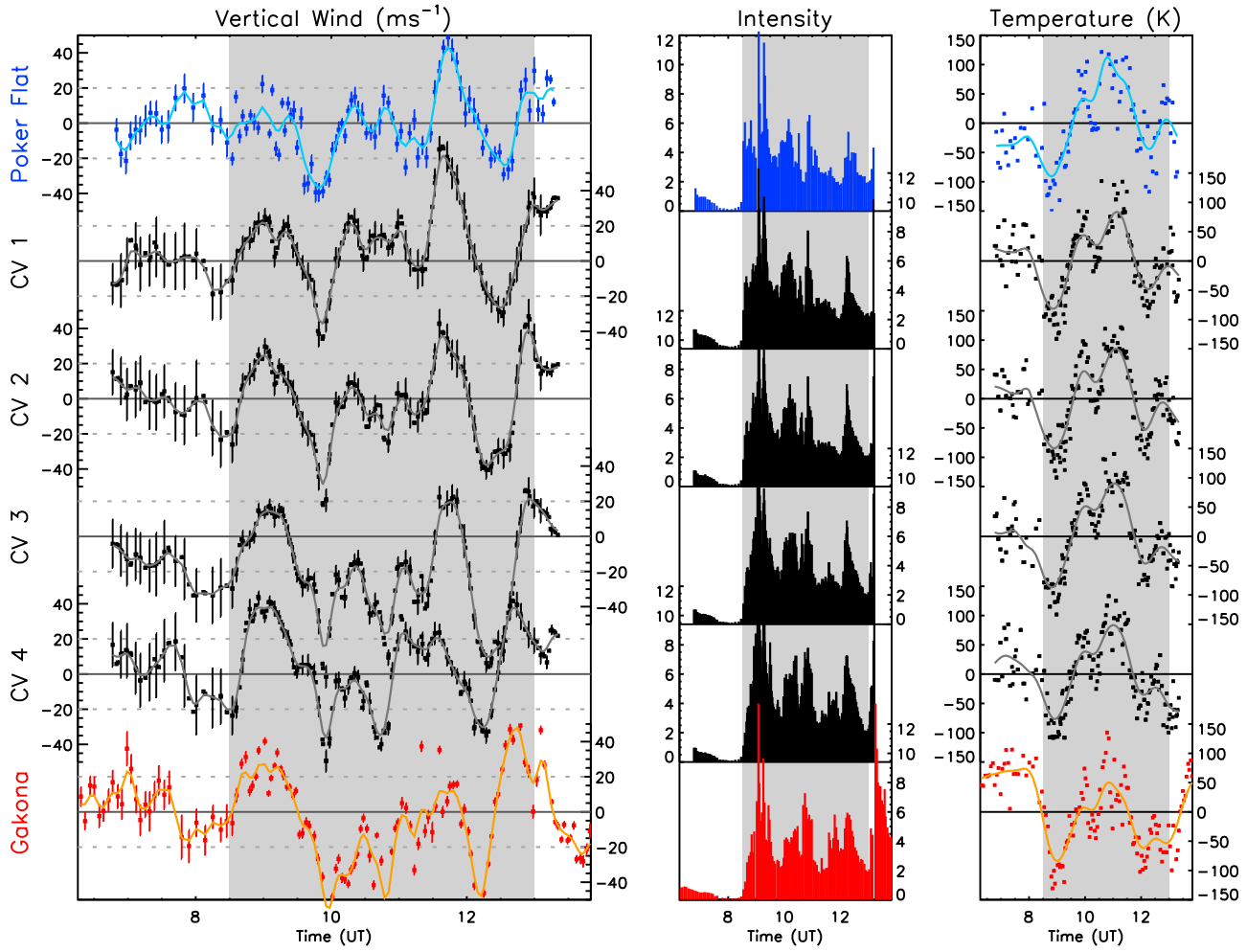


**Figure 3.** Vertical winds, intensities and temperatures on April 5, 2010. Plot format is the same as Figure 2. Median temperature uncertainty was 15 K.

mean temperature at each location) are shown in Figure 4. These panels are displayed similarly to Figure 3, with the addition of Fort Yukon and Gakona magnetometer measurements of the horizontal magnetic field strength in the top and bottom panels respectively (magnetometer data from Poker Flat were not available for this time period). This figure shows that the beginning of the vertical wind disturbances were approximately concurrent with the very large increase in magnetic field strength near 0830 UT.

[35] Between approximately 0830 and 1130 UT the observed temperature oscillations were anti-correlated with the vertical wind fluctuations. This relationship would be expected if the cause of the disturbance was an atmospheric gravity wave. After 1130 UT there appeared to be a change in the phase relationship between the temperature and vertical wind oscillations. Above Gakona and in CV's 3 and 4 (i.e. closer to the auroral oval) the temperature and vertical wind fluctuations were approximately in-phase, while toward Poker Flat there was still a time lag with temperature fluctuations leading vertical wind fluctuations.

### 4.3. April 7, 2010

[36] Data for April 7, 2010 are shown in Figure 5. Two periods of interest are highlighted for this night. A peak in auroral brightness was observed at approximately 0830 UT. Prior to this intensity peak upward winds of ~20 m s$^{-1}$ were observed above Poker Flat and in CV's 2 and 4. Following the intensity peak a correlated downward wind of magnitude 10–40 m s$^{-1}$ was seen at all locations between 0900–0915 UT. A small time-lag of approximately 20 min separated the peak downward wind, which was observed first at Poker Flat, and last above Gakona.

[37] Temperature oscillations of ~20–50 K were observed concurrently with the vertical winds during this period, with a similar time lag. These oscillations were again anti-correlated with the direction of the vertical winds: negative temperature perturbations prior to the intensity peak (except above Poker Flat), positive perturbations after the peak. Although not clear in the vertical wind data, the temperature data suggest that the oscillations may have started approximately 30 min to an hour earlier than the start of the shaded region in Figure 5, near an earlier intensity peak.

[38] The second period of interest also coincided with elevated intensities. At the beginning of this period downward winds were observed above Gakona, and, at progressively later times, this downward wind was also observed in the CV's northward of Gakona. It was observed above Poker Flat at 1200 UT, approximately 1.5 hours after it was seen

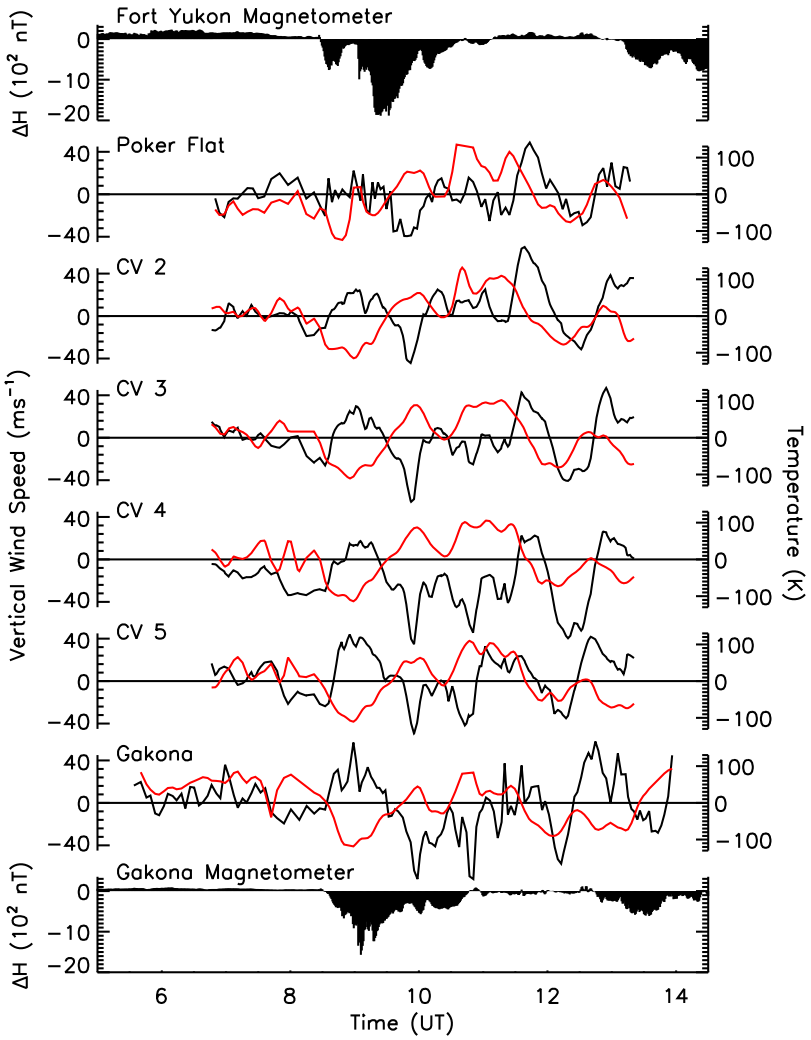


**Figure 4.** Vertical winds (black) and temperatures (red) on April 5, 2010, superimposed (middle six panels). Temperatures have been smoothed with a 4 minute half-width Gaussian window. The top and bottom panels show variations in the horizontal component of the magnetic field, as measured from (top) Fort Yukon and (bottom) Gakona.

above Gakona. Following the downward wind, upward winds were observed above Poker Flat and in CV's 1 and 2, while in CV 3 the wind abated. In CV 4 an upward wind of 20 m $s^{-1}$ was observed after a small-magnitude up-down oscillation, while above Gakona no significant vertical winds were observed.

[39] The temperature perturbations during this period did not show clear oscillatory behavior as they did during the previous period of interest, however small oscillations were present above Poker Flat and in CV 1, where the clearest oscillatory behavior was also observed in the vertical winds. All locations observed an increasing temperature during or following this time period.

### 4.4. December 8, 2010

[40] Vertical winds from December 8, 2010 are shown in Figure 6. The main feature of the vertical wind on this night was a correlated, large-scale wind oscillation beginning at 0300 UT with upward winds that peaked at approximately 0430 UT. CV's 1 and 2 did not observe significant upward winds at this time, however they did observe a clear reduction in downward wind speed just prior to 0430 UT. The upward wind was followed by a downward wind that was observed in all locations, and which peaked around 0700 UT with a magnitude of approximately 20 m $s^{-1}$. Upward winds of ~20 m $s^{-1}$ were observed again following the downward wind, however these winds were most clearly observed above Poker Flat and in the common-volumes. Above Gakona the average wind was positive, but no clear upward wind peak was observed.

[41] The highest intensities were observed above Poker Flat during this time period, with intensity decreasing with decreasing latitude. All-sky images showed the auroral oval visible on the magnetic northward edge of the Poker Flat field-of-view. There was appreciable scatter in the temperatures measured on this night, likely due to the relatively lower intensities, and thus no significant temperature

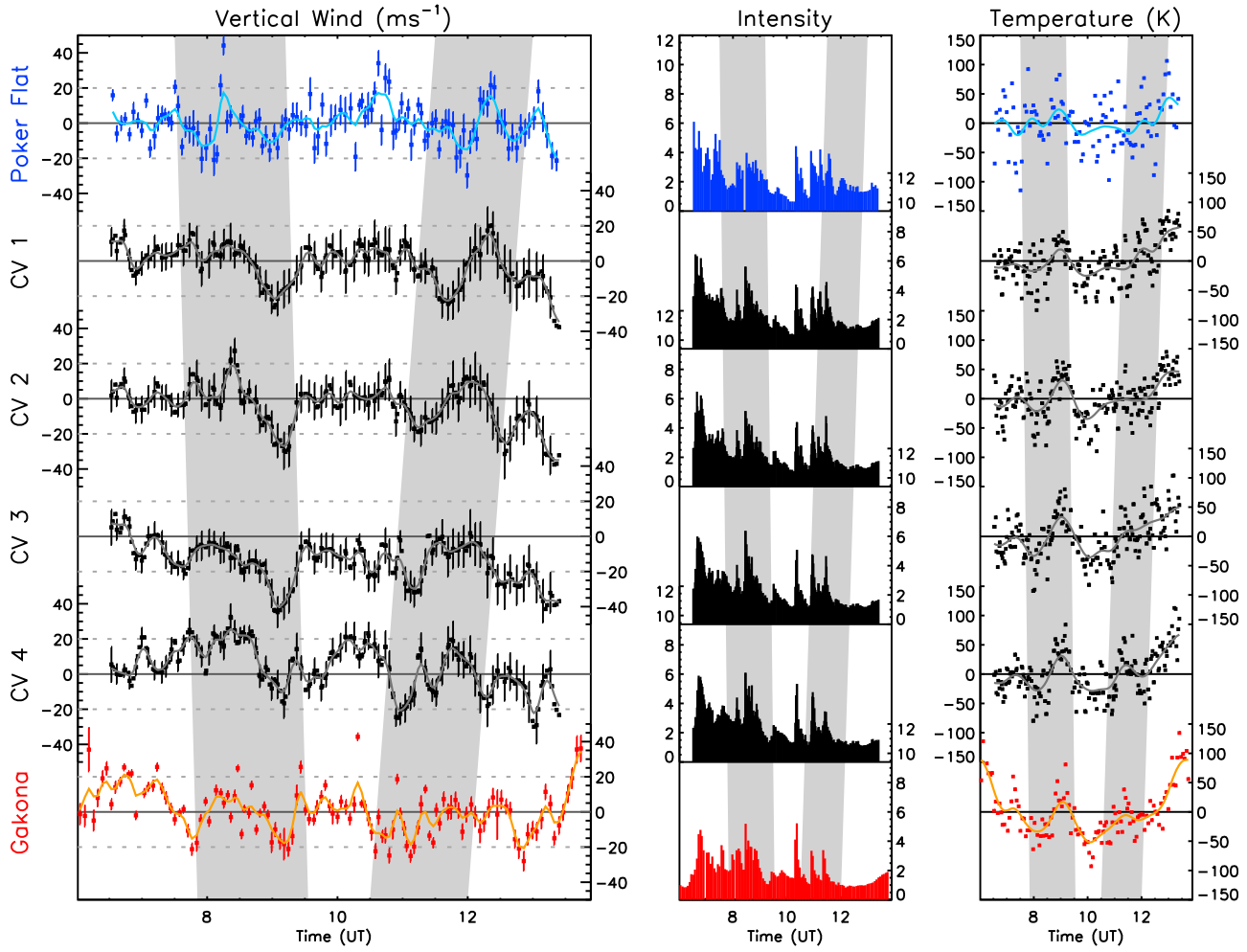


**Figure 5.** Vertical winds, intensities and temperatures on April 7, 2010. Plot format is the same as Figure 2. Median temperature uncertainty was 20 K.

oscillations were observed, nor any significant correlation between the temperature and vertical wind fluctuations.

## 5. Discussion

### 5.1. Vertical Wind Distribution

[42] The distribution of vertical winds observed in this study is shown in Figure 7. For this figure data have been included from all bistatic locations in addition to the station zenith measurements, and data have been included from the entire 19-night data set. Percentage values indicate the total occurrence frequency within the given dashed lines. For the current data set, 99.3% of measured vertical winds had magnitudes less than 50 m s$^{-1}$, and 93.5% had magnitudes less than 30 m s$^{-1}$. This compares well with the distributions presented by *Conde and Dyson* [1995] and *Greet et al.* [2002], however the distribution in the present study shows significantly fewer observations of vertical winds with magnitudes greater than 50 m s$^{-1}$, compared to the studies just cited.

[43] Approximately 1% of all upward vertical winds observed in the current study had speeds in excess of 50 m s$^{-1}$, while 0.6% of all downward winds had speeds more negative than -50 m s$^{-1}$, indicating that fast upward winds were approximately twice as frequent as fast downward winds (however both types of winds were very rare in an absolute sense). For speeds of >100 ms$^{-1}$, the ratio of upward to downward wind events was 2.4 (12.1% upward, 5.1% downward). Observations of large vertical winds reported in the literature (see references in the introduction) have almost exclusively been of upward winds, and while vertical winds in excess of 50 m s$^{-1}$ were observed very infrequently in the current data set, the statistical distribution certainly supports the more frequent occurrence of large upward winds relative to downward winds.

[44] The red curve in Figure 7 shows a Gaussian fitted to the observed histogram. The fitted Gaussian profile had a mean of $\mu = -0.63(\pm 0.03)$ m s$^{-1}$ and standard deviation of $\sigma = 15.25(\pm 0.03)$ m s$^{-1}$, which are indicated in the plot. The Gaussian peak height (not shown) was 5.15(±0.01)%. *Conde and Dyson* [1995] derived vertical wind standard deviations of 22.4 m s$^{-1}$ (local K-index < 3) and 24.9 m s$^{-1}$ (local K-index ≥ 3) from one year of data at Mawson (these values were the raw sample deviations, before attempting to account for the broadening effect of measurement uncertainties). *Greet et al.* [2002], using four years of data from Mawson and Davis stations, derived standard deviations from fitted Gaussian profiles and obtained values of

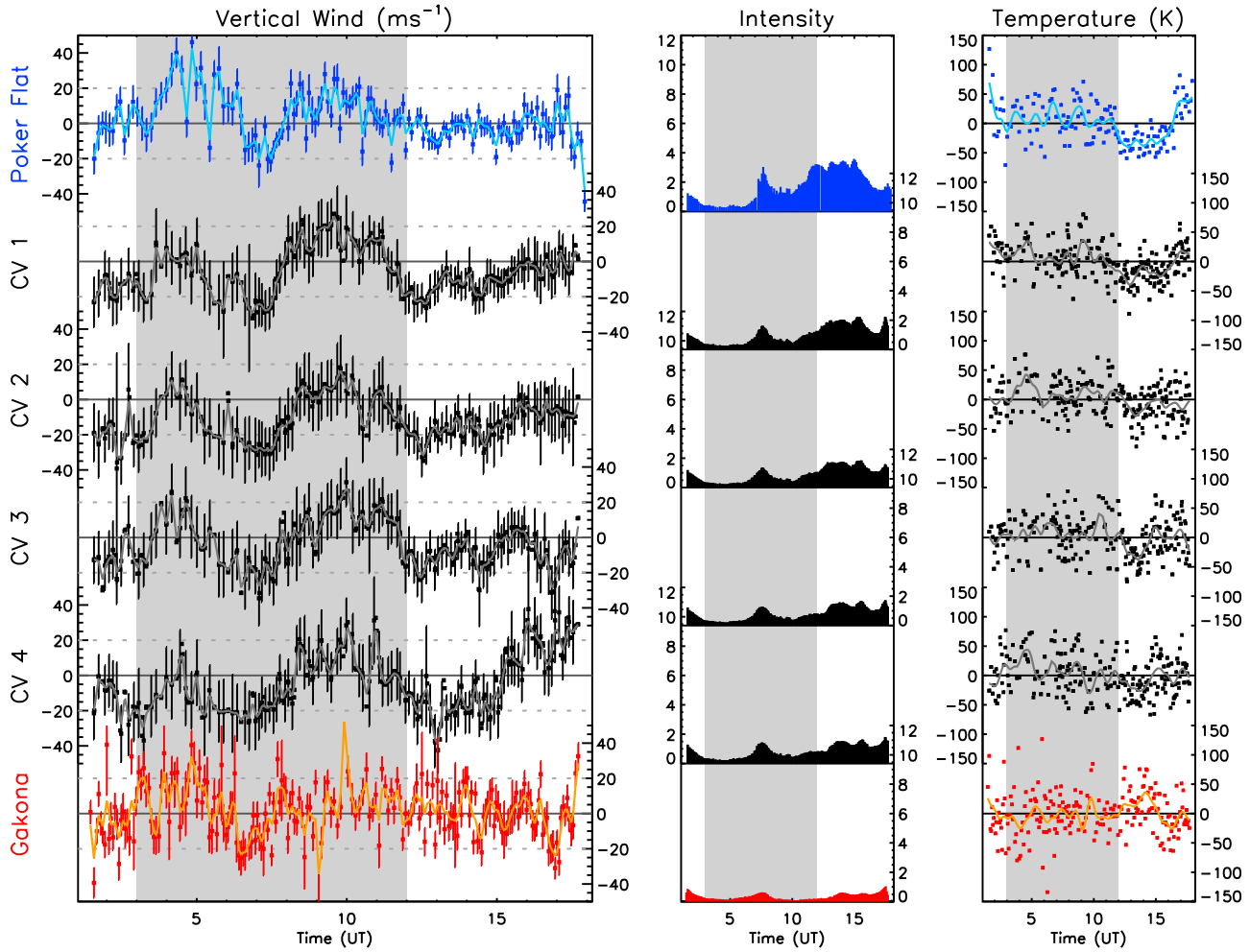


**Figure 6.** Vertical winds, intensities and temperatures on December 8, 2010. Plot format is the same as Figure 2. Median temperature uncertainty was 25 K.

25.13(±0.02) m s$^{-1}$ at Davis and 19.99(±0.02) m s$^{-1}$ at Mawson.

[45] These earlier studies were carried out in the southern hemisphere at Mawson [*Conde and Dyson*, 1995] and Davis [*Greet et al.*, 2002] stations in Antarctica. Both of these stations are at higher magnetic latitudes than Poker Flat, which was the highest latitude location in the present work. Large-magnitude vertical winds are more frequently observed at higher magnetic latitudes [e.g., *Spencer et al.*, 1982], thus the smaller vertical wind standard deviation observed in the current work is possibly due to the different geomagnetic latitudes sampled.

[46] Note that while the mean downward vertical wind of − 0.63 observed in the present study is statistically significant (it is approximately 6 times larger than the standard error), no attempt has been made to account for the (possibly asymmetric) influence of experimental uncertainties on the observed distribution. In addition, the nightly mean vertical wind at each station is set equal to zero in order to derive line-of-sight Doppler velocities from measured airglow spectra. Thus this result almost certainly reflects the (relatively) larger uncertainties associated with the bistatic measurement of vertical winds, and therefore we do not attach any physical significance to it.

[47] Vertical wind distributions have also been derived separately in each observing volume (not shown). No systematic trend was observed in the standard deviations (or means) as a function of (for example) magnetic latitude, however distributions from the bistatic locations were typically broader than those from the station zeniths, presumably due to the larger uncertainties associated with the bistatic inversion. The lack of a clear latitudinal trend in the distribution standard deviation may indicate that the geomagnetic latitudinal resolution of the sampling was too fine relative to the average width and variability of the auroral oval. This is reasonable given that the largest magnetic latitudinal separation in the current data set is ∼ 2.4°.

### 5.2. Spatial Correlation

[48] Horizontal scale lengths of the observed vertical winds were investigated as follows. For a given night, vertical wind time series (both station zenith and bistatic) were linearly interpolated to a common, evenly spaced time grid. The time-dependent linear Pearson correlation coefficient between every pair of vertical wind locations (2 station zenith and 4 bistatic locations, 15 pairs in all) was calculated within a sliding window of 1 hour half-width. All correlations were calculated using zero time-lag between the data

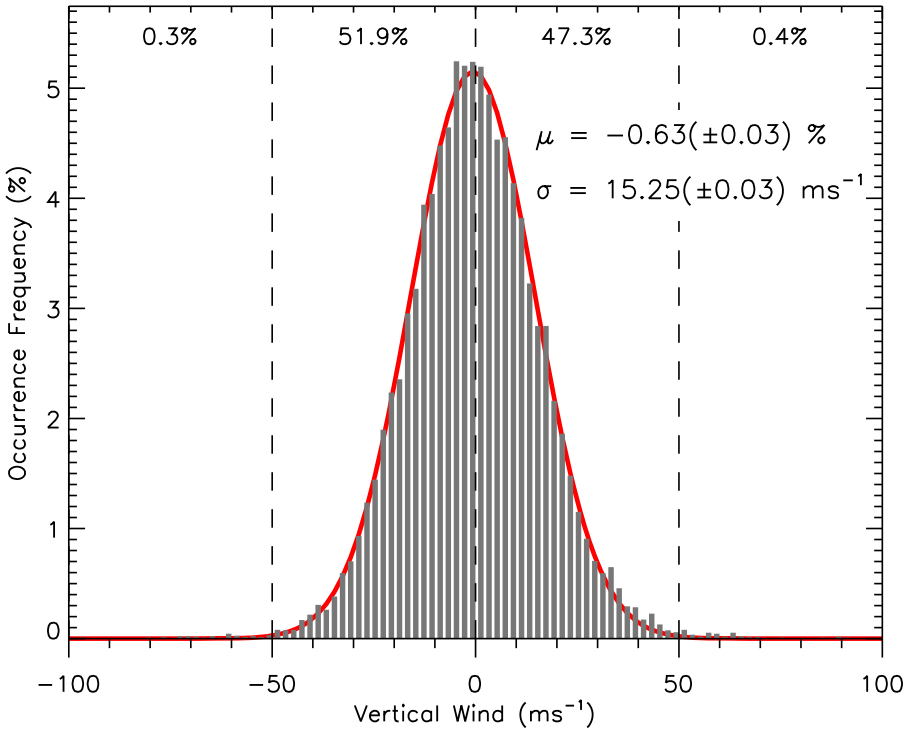


**Figure 7.** Occurrence frequency distribution of vertical winds measured at all locations (station zenith and bistatic). Percentages listed at the top of the figure indicate the total occurrence frequency within the dashed lines. The vertical wind bin width is 2 m $s^{-1}$. A Gaussian fitted to the distribution is shown by the red curve, and the mean ($\mu$) and standard deviation ($\sigma$) of the fitted curve are shown.

subsets. The width of the sliding window was chosen to reduce the effect of measurement noise (by averaging over many samples) and to capture the time-scales of the vertical wind features that are most commonly observed.

[49] For every calculated correlation coefficient the statistical significance was estimated using the Student's t-test. To estimate the number of degrees of freedom within a given time window, the number of raw samples from each of the Gakona and Poker Flat SDI's within that time-window was averaged to give an estimate of the number of unique data points ($N$). The number of degrees of freedom was estimated by $N - 2$, and the two-tailed significance (i.e. allowing for both positive and negative correlation between the samples) was calculated using the Student's t-test, giving the statistical confidence level that the observed correlation coefficient did not arise from uncorrelated samples.

[50] The time-dependent correlations between all vertical wind location pairs from all available nights of data (19 nights in all) were then sorted by the horizontal separation between the locations into separation bins of width 50 km. Within each bin, the fraction of $r$ values for which the significance was greater than 90% was calculated. We thereby determined the occurrence frequency of (statistically significant) correlated vertical wind estimates as a function of the baseline separation between the vertical wind measurement locations. These data are shown as solid black squares in Figure 8 (top). For comparison, the data have additionally been sorted by *ap* index, and these data are shown as blue diamonds ($ap < 3$) and red crosses ($ap > 20$) respectively. The lower panel indicates the total number of $r$ values within each separation bin.

[51] A straight-line fit to the data (under all levels of activity, shown by the black squares) is shown by the solid line in Figure 8, with the equation of the line and coefficient of determination shown at the bottom of the plot. Values in brackets indicate the 1-$\sigma$ uncertainties. The quality of the fitted linear model indicates that approximately 98.5% of the variation in the occurrence frequency was explained by the increasing separation. Thus we conclude that for the available data set the chance of observing statistically significant correlation between vertical winds measured at two locations decreased linearly with increasing separation between those locations (at the rate of ~0.13 percent per kilometer), at least over the range of separations sampled in this study.

[52] Assuming that the linear model remains valid at larger and smaller separations, we can estimate the smallest horizontal separation beyond which no statistically significant correlation between vertical wind estimates would be expected (i.e. an upper limit on the correlation length). For the given data set this separation is equal to ~540 km. Extrapolating the linear model back to zero separation indicates that significant correlation would be expected only 68% of the time. The active-time data in Figure 8 (red crosses) suggest that the linear trend may not be valid under enhanced levels of geomagnetic activity. While there is insufficient active data to be confident in this result, it would be worthwhile to investigate this with a more comprehensive data set.

[53] It is important to realize that the statistical significance of the correlation coefficient depends on the amplitude of the underlying signal relative to the magnitude of the

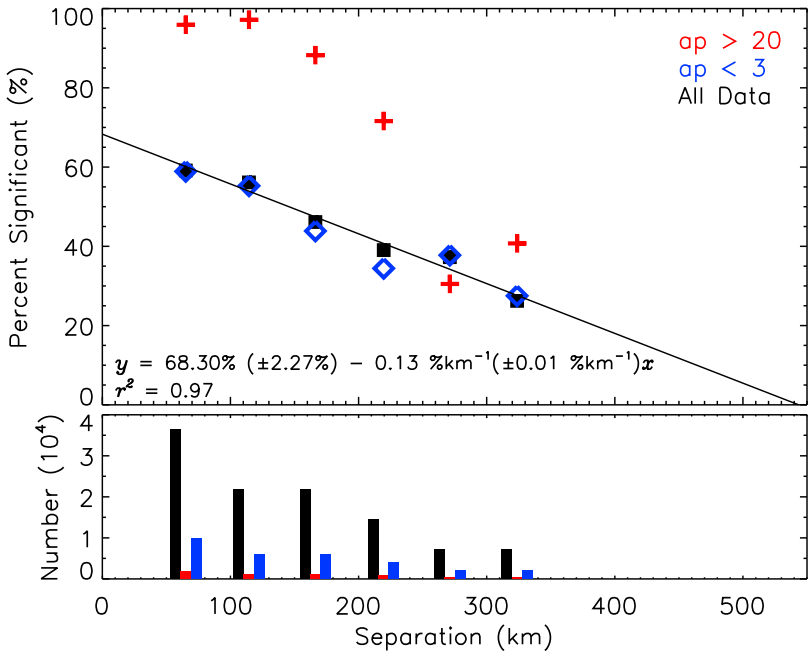


**Figure 8.** (top) Filled black squares show the probability of observing a significant vertical wind correlation at locations separated by the given distance, under all levels of activity. Blue diamonds and red crosses show the result when the data are filtered for low ($ap < 3$) and 'high' ($ap > 20$) geomagnetic activity respectively. The straight line shows a linear fit to the entire data set (black squares), with the fitted equation and coefficient of determination indicated at the bottom of the plot. (bottom) The number of observations within each separation bin.

experimental uncertainty. We have calculated the signal amplitude for which the fraction of statistically significant correlation coefficients is reduced to 68%, by creating a sinusoidal vertical wind variation, and adding random noise to simulate two separate measurements of this same signal. Generated noise had a standard deviation of 10 m s$^{-1}$, equal to the median common-volume vertical wind uncertainty in Figures 2, 3, 5, and 6. In the presence of this level of noise, the two estimates of the same underlying signal produce significant correlation 68% of the time when the signal amplitude is approximately 6 m s$^{-1}$. From the distribution shown in Figure 7, we calculate that vertical winds of magnitude less than 6 m s$^{-1}$ are observed approximately 30% of the time. Thus we conclude that while the chance of observing significant correlation at zero separation is approximately 68%, what this number really indicates is the frequency at which vertical winds of sufficiently large magnitude (to produce a significant correlation) are observed.

[54] The above estimate of 540 km as the largest horizontal correlation length only strictly applies along the direction of the Gakona/Poker Flat great circle, since vertical winds were only resolved along this direction. In addition, it must be pointed out that because the analysis made no use of a time-lag between samples, and was averaged over many nights, it will be less sensitive to contributions from propagating waves, unless the phase-fronts of those waves are aligned approximately parallel to the Gakona/Poker Flat great circle (and therefore produce correlated vertical winds at zero time lag). Likewise, vertical winds advected into the field-of-view by horizontal winds would only produce a correlated response if the direction of the horizontal wind was approximately perpendicular to the Gakona/Poker Flat great circle.

[55] Given that two of the most likely sources of vertical winds at auroral latitudes are heating from Joule dissipation and particle precipitation, it is reasonable to assume that in-situ vertical wind-forcing would often be aligned parallel to the auroral oval. The direction of the Gakona/Poker Flat great circle is approximately 40° west of magnetic north (defined by the direction perpendicular to the nominal auroral oval at 240 km altitude), and therefore approximately 50° east of the direction parallel to the auroral oval. Therefore it is also likely that the estimate of 540 km for the maximum correlation length is a mid-range estimate, and that a similar estimate made using a geomagnetic longitudinal baseline might produce a larger correlation length. Conversely, a predominantly geomagnetic latitudinal baseline might be expected to produce a smaller correlation length.

[56] The horizontal scale length derived here is qualitatively consistent with previous estimates of the horizontal spatial scales of thermospheric vertical winds (see Table 1). Comparison with these previous studies is complicated by the different locations (small changes in average proximity to the auroral oval might strongly affect the horizontal scales), different baseline orientations, different levels of prevailing geomagnetic and solar activity, and the poorly understood influence of waves.

[57] As a case in point, the most directly comparable study to the current work was reported by *Anderson et al.* [2011].

**Table 1.** Survey of Estimated Vertical Wind Horizontal Correlation Lengths

| Correlation Length (km) | Altitude (km) | Reference | Comment |
|---|---|---|---|
| <800 | 240 | *Price et al.* [1995] | Estimated from a single station |
| 500 | 300-500 | *Spencer et al.* [1982] | DE-2, geographic north-south baseline, variable altitude |
| 360 | 240 | *Crickmore* [1993] | Estimated from a single station |
| 150-480 | 240 | *Anderson et al.* [2011] | Variable correlation, 60° away from magnetic east-west baseline |
| ~300 | 240 | *Ishii et al.* [2004] | Weakly correlated, magnetic east-west baseline |
| <45 | 240 | *Kosch et al.* [2000] | Essentially no correlation, magnetic east-west baseline |

This study was carried out in the southern hemisphere, between Mawson and Davis stations in Antarctica, along a baseline directed approximately 30° east of geomagnetic south. The lowest absolute geomagnetic latitude sampled in that study was 70°, approximately 4° higher than the highest sampled latitude in the present work (66° at Poker Flat). The correlation between adjacent common-volumes in the *Anderson et al.* [2011] study was significantly lower than was observed in the present work, except during isolated (in time) disturbances. The differing magnetic latitudes, levels of geomagnetic activity, and baseline orientation relative to the auroral oval may all contribute to different observed frequencies of correlated vertical winds.

[58] The <70% chance of observing significant correlation at separations smaller than 50 km (indicated by the linear model) suggests that observations such as those reported by *Kosch et al.* [2000] should occur relatively infrequently, but does not rule them out. The majority of previous scale size estimates lie in the range of 300–500 km. From the linear model presented here, at 300 km separation we would expect to see correlated vertical winds approximately 30% of the time. At 500 km separation, the predicted frequency would drop to negligible levels (3%).

[59] We note that the correlation scale length estimates reported here are based on a larger vertical wind data set than those in the studies shown in Table 1, and on a more comprehensive sampling of the spatial variation of the vertical wind field (with the possible exception of the *Anderson et al.* [2011] study, however the temporal resolution of the underlying data in that study were not as high as in the present work). These two factors allowed us to apply extra restrictions on the data, such as requiring that a correlation be statistically significant above the 90% level to be considered for inclusion. Thus we believe that the values reported here are firm estimates of the spatial correlation length, with the caveats discussed above.

### 5.3. Factors Affecting Spatial Correlation

[60] One way in which line-of-sight wind speed estimates may be coupled between different viewing zones (of a single instrument) is through drift correction. This correction is intended to remove the effect of small changes in optical path length through the etalon during the course of a night (due, for example, to changes in etalon plate separation), which can affect wind speed estimates by changing the apparent peak wavelength of sky spectra. The wavelength shift due to a change in etalon plate separation should be constant across all zones, and therefore a single drift curve is effectively subtracted from the winds estimated in each zone. An incorrect estimate of the etalon drift might therefore introduce artifacts into the winds derived in all zones, thereby coupling them.

[61] Instrumental drift is tracked by the change in inferred peak wavelength of a frequency-stabilized calibration laser throughout the night. The laser wavelength is assumed constant (at the resolution of the spectrometer), and therefore changes in inferred calibration wavelength are attributed to variations in optical path length through the etalon. The character of the instrumental drift is similar for both instruments. By far the largest component of the drift is a gradual, nearly monotonic, change in inferred calibration wavelength over the course of the night.

[62] The drift-correction algorithm converts the change in inferred calibration wavelength into an equivalent change in wind speed at the sky wavelength of interest. The magnitude of the equivalent change in wind speed caused by the gradual component of the drift differs between the two instruments; at Poker Flat, it is between ~10–50 m $s^{-1}$, while at Gakona, the magnitude is frequently in the range ~50–150 m $s^{-1}$. These changes occur on time-scales of several hours (e.g. 5 hours or more), and are easily handled by the drift-correction algorithm, which reduces these drifts to just a few m $s^{-1}$.

[63] Shorter-period (~30 min for the Gakona SDI and ~2 hours for the Poker Flat SDI) oscillations with equivalent magnitudes of less than 10 m $s^{-1}$ are sometimes observed superposed on the gradual component of the drift. These oscillations are believed to be due to the thermal control units that attempt to maintain a constant temperature within the etalon housing. The different time-scales are likely due to the physical environments of the two instruments. The Poker Flat SDI is located in a large building, while the Gakona SDI operates from a small heated trailer that is parked outside. The thermal time-constants of the former would very likely be longer than those of the latter, hence leading to a longer-period thermal control cycle.

[64] Thus not only are the drift time-constants different between the two instruments, and the drifts themselves small in magnitude, but in order to produce a correlated vertical wind response in the zenith data, the drifts between the two instruments would have to be correlated, which is highly improbable. From these considerations it is very unlikely that the spatially correlated structures observed in the bistatic vertical winds presented here were due to coupling as a result of instrumental drift correction. Another possible cause of large-scale correlation is heavy cloud within the field-of-view. If a bright auroral arc was present in addition to heavy cloud cover, then the dominant auroral signal could be scattered into each viewing direction, in which case the line-of-sight winds from spatially separate locations could be highly correlated.

[65] Fortunately it is relatively easy to identify periods of heavy cloud cover from time series of all-sky average wind components, and to reject such periods from analysis. Partial or light cloud cover is more difficult to identify, however the

corresponding influence on the data would be reduced (and again it would typically affect each site differently). Thus, while the influence of partial or light cloud cover cannot be ruled out, it is unlikely that this would greatly affect the interpretation of these data.

### 5.4. Waves

[66] The vertical wind (and often temperature) time series shown here frequently displayed wave-like oscillations, and on two nights (January 24 and April 7) there were instances of vertical wind disturbances that appeared to be systematically time-lagged between the locations at which they were observed. These types of behavior were observed throughout the entire data set. Discrete vertical wind disturbances that are observed at later times at higher/lower latitudes may be due to vertical winds being advected through the common-volume by the horizontal wind, or to a moving source of in-situ heating. Oscillatory-type behavior is probably due to atmospheric gravity waves.

[67] The winds observed on April 5, 2010 were an exceptional example of these wave-like oscillations, with vertical wind and temperature amplitudes reaching $\sim$50 m s$^{-1}$ and $\sim$100 K respectively. Vertical winds of this magnitude were only rarely observed in the current data set (see Figure 7). The magnetic perturbations measured at Fort Yukon on this night were very large, up to 2000 nT in magnitude, which is exceptionally large in comparison with recent levels of magnetic activity.

[68] Very high levels of geomagnetic activity should be conducive to the observation of gravity waves for two reasons. First because of enhanced geomagnetic energy sources such as Joule and particle heating, which are likely to be important gravity wave sources. Secondly, enhanced geomagnetic activity typically results in a larger auroral oval, which increases the likelihood that a given station will be located within the geomagnetic polar cap (i.e. poleward of the auroral oval). It is in this region that vertical wind oscillations are most likely to be observed [*Innis and Conde*, 2002]. Thus conditions on the night of April 5, 2010 were very favorable for observing gravity waves, as the auroral oval was equatorward of Gakona for the time period displayed in Figure 3, and geomagnetic activity (as measured by the magnetometer) was greatly enhanced.

[69] Recently, *Knipp et al.* [2011] have observed instances of very large Earth-directed Poynting flux exceeding 170 mW m$^{-2}$ in the dayside cusp region. Extreme values of Poynting flux were associated with a large east-west component of the interplanetary magnetic field (IMF $B_y$), and indicated that even during nominally quiet times (in terms of geomagnetic storm indices) the high-latitude dayside thermosphere can receive significant energy input. These observations were consistent with observations of high neutral density structures in the dayside cusp associated with large IMF $B_y$ [*Crowley et al.*, 2010]. Modeling [e.g., *Demars and Schunk*, 2007] has suggested that these density enhancements are associated with neutral upwelling and heating, and therefore may constitute a dayside source of gravity waves. Simultaneous measurements of neutral thermospheric wind and Poynting flux would be required to confirm this.

[70] Estimation of wave properties such as horizontal wavelength and propagation direction was not attempted in the present work. With only one unique baseline orientation (the direction of the Gakona/Poker Flat great circle), estimation of these properties from the vertical wind data alone is not possible. A more in-depth analysis would need to investigate perturbations to the line-of-sight wind estimates from all look-directions. Alternatively, the addition of a third SDI to produce a tristatic array would allow for unambiguous three-component wind vector estimation in the common-volumes, from which wave parameters could be estimated directly.

## 6. Conclusion

[71] Bistatic inversion of common-volume line-of-sight wind observations between two scanning Doppler imagers in Alaska have been used to infer vertical winds at four locations along the Gakona/Poker Flat great circle in addition to the vertical winds routinely estimated in each station's zenith. The main results of this analysis are summarized below:

1. Observed vertical wind magnitudes at all locations were rarely larger than 50 m s$^{-1}$, and 93.5% of vertical winds from all 19 nights in the current data set had magnitudes less than 30 m s$^{-1}$. The distribution of vertical winds was approximately Gaussian, with a peak height of 5.15($\pm$0.01)%, mean of $-$0.63($\pm$0.03) m s$^{-1}$, and standard deviation of 15.25($\pm$0.03) m s$^{-1}$ (however the true vertical wind distribution may be narrower than this, due to the effect of measurement uncertainty).

2. The frequency of statistically significant correlation between vertical winds measured at separate locations decreased approximately linearly with increasing separation. This relationship was well modeled by the linear function

$$y = 68.30\%\ (\pm 2.27\%) - 0.13\%\ \mathrm{km}^{-1}\left(\pm 0.01\%\ \mathrm{km}^{-1}\right)x \quad (1)$$

where $y$ is the (percentage) frequency of occurrence and $x$ is the horizontal separation between measurement locations measured in kilometers. This model was strictly only valid for separations between $\sim$50–330 km, and for baselines making an angle of approximately 50° with the direction tangent to the nominal auroral oval.

3. By assuming the linear model to be valid at separations greater than 330 km, we estimated that the largest separation over which (statistically significant) correlated vertical winds would be observed is $\sim$540 km. At zero separation, where correlation should occur 100% of the time, the linear model predicted a frequency of $\sim$68%, which was interpreted as indicating the frequency with which sufficiently large (to produce a statistically significant correlation) vertical winds were observed.

4. The relatively frequent occurrence of wave-like oscillations and vertical wind disturbances that were systematically time-lagged with respect to geomagnetic latitude indicated the presence of propagating gravity waves. Because the correlation analysis did not consider time lags, the frequency of occurrence of correlated winds may be substantially higher if lags associated with propagating waves were accounted for. Estimation of wave parameters could be achieved by examining perturbations to the line-of-sight winds measured in all look-directions, or by the addition of a third SDI to form a tristatic array.

[72] Future work will aim to identify and characterize the frequently observed oscillations, through the use of multiple look directions. In addition, there are plans to install two more scanning Doppler imagers in Alaska, at Toolik Lake and Kaktovik. The addition of these two instruments to the current pair would provide a unique opportunity to map the vertical wind field with good spatial resolution from the northern coast of Alaska down to Gakona, spanning approximately 7° of latitude, and to monitor this wind field with high temporal resolution. In addition, tristatic sampling in limited areas of field-of-view overlap will increase the dimensionality (from 1 to 2 dimensions) and spatial coverage of the vertical wind mapping, in addition to allowing unambiguous determination of the three-component wind vector.

[73] **Acknowledgments.** Gakona SDI installation and operations were supported by Carl Andersen, Tim Manning, and Marty Karjala. Poker Flat SDI operations were supported by Carl Andersen, Don Hampton, and Brian Lawson. The authors gratefully acknowledge the assistance provided by these individuals.

[74] Robert Lysak thanks the reviewers for their assistance in evaluating this paper.

## References

Anderson, C., T. Davies, M. Conde, P. Dyson, and M. J. Kosch (2011), Spatial sampling of the thermospheric vertical wind field at auroral latitudes, *J. Geophys. Res.*, *116*, A06320, doi:10.1029/2011JA016485.

Anderson, C., M. Conde, and M. G. McHarg (2012), Neutral thermospheric dynamics observed with two scanning Doppler imagers: 1. Monostatic and bistatic winds, *J. Geophys. Res.*, *117*, A03304, doi:10.1029/2011JA017041.

Aruliah, A. L., and D. Rees (1995), The trouble with thermospheric vertical winds: geomagnetic, seasonal and solar cycle dependence at high latitudes, *J. Atmos. Terr. Phys.*, *57*(6), 597–609.

Biondi, M. A. (1984), Measured vertical motion and converging and diverging horizontal flow of the midlatitude thermosphere, *Geophys. Res. Lett.*, *11*(1), 84–87.

Biondi, M. A., and D. P. Sipler (1985), Horizontal and vertical winds and temperatures in the equatorial thermosphere: Measurements from Natal, Brazil during August–September 1982, *Planet. Space Sci.*, *7*(7), 817–823.

Burnside, R. G., F. A. Herrero, J. W. Meriwether Jr., and J. C. G. Walker (1981), Optical observations of thermospheric dynamics at Arecibo, *J. Geophys. Res.*, *86*, 5532–5540.

Conde, M., and P. L. Dyson (1995), Thermospheric vertical winds above Mawson, Antarctica, *J. Atmos. Terr. Phys.*, *57*(6), 589–596.

Crickmore, R. I. (1993), A comparison between vertical winds and divergence in the high-latitude thermosphere, *Ann. Geophys.*, *11*(8), 728–733.

Crickmore, R. I., J. R. Dudeney, and A. S. Rodger (1991), Vertical thermospheric winds at the equatorward edge of the auroral oval, *J. Atmos. Terr. Phys.*, *53*(6–7), 485–492.

Crowley, G., D. J. Knipp, K. A. Drake, J. Lei, E. Sutton, and H. Lühr (2010), Thermospheric density enhancements in the dayside cusp region during strong $B_y$ conditions, *Geophys. Res. Lett.*, *37*, L07110, doi:10.1029/2009GL042143.

Demars, H. G., and R. W. Schunk (2007), Thermospheric response to ion heating in the dayside cusp, *J. Atmos. Sol. Terr. Phys.*, *69*, 649–660.

Deng, Y., and A. J. Ridley (2007), Possible reasons for underestimating Joule heating in global models: *E* field variability, spatial resolution, and vertical velocity, *J. Geophys. Res.*, *112*, A09308, doi:10.1029/2006JA012006.

Deng, Y., A. D. Richmond, A. J. Ridley, and H.-L. Liu (2008), Assessment of the non-hydrostatic effect on the upper atmosphere using a general circulation model (GCM), *Geophys. Res. Lett.*, *35*, L01104, doi:10.1029/2007GL032182.

Fuller-Rowell, T. J. (1985), A two-dimensional, high-resolution, nested-grid model of the thermosphere: 2. response of the thermosphere to narrow and broad electrodynamic features, *J. Geophys. Res.*, *90*(A7), 6567–6586.

Fuller-Rowell, T. J., and D. Rees (1980), A three-dimensional time-dependent global model of the thermosphere, *J. Atmos. Sci.*, *37*, 2545–2567.

Greet, P. A., J. L. Innis, and P. L. Dyson (2002), Thermospheric vertical winds in the auroral oval/polar cap region, *Ann. Geophys.*, *20*, 1987–2001.

Guo, W., and D. J. McEwen (2003), Vertical winds in the central polar cap, *Geophys. Res. Lett.*, *30*(14), 1725, doi:10.1029/2003GL017124.

Hernandez, G. (1982), Vertical motions of the neutral thermosphere at midlatitude, *Geophys. Res. Lett.*, *9*(5), 555–557.

Innis, J. L., and M. Conde (2002), High-latitude thermospheric vertical wind activity from Dynamics Explorer 2 wind and temperature observations: Indications of a source region for polar cap gravity waves, *J. Geophys. Res.*, *107*(A8), 1172, doi:10.1029/2001JA009130.

Innis, J. L., P. A. Greet, and P. L. Dyson (1996), Fabry-Perot spectrometer observations of the auroral oval/polar cap boundary above Mawson, Antarctica, *J. Atmos. Terr. Phys.*, *58*(16), 1973–1988.

Innis, J. L., P. A. Greet, D. J. Murphy, M. G. Conde, and P. L. Dyson (1999), A large vertical wind in the thermosphere at the auroral oval/polar cap boundary seen simultaneously from Mawson and Davis, Antarctica, *J. Atmos. Sol. Terr. Phys.*, *61*, 1047–1058.

Ishii, M. (2005), Relationship between thermospheric vertical wind and the location of ionospheric current in the polar region, *Adv. Polar Upper Atmos. Res.*, *19*, 63–70.

Ishii, M., S. Oyama, S. Nozawa, R. Fujii, E. Sagawa, S. Watari, and H. Shinagawa (1999), Dynamics of neutral wind in the polar region observed with two fabry-perot interferometers, *Earth Planets Space*, *51*, 833–844.

Ishii, M., M. Conde, R. W. Smith, M. Krynicki, E. Sagawa, and S. Watari (2001), Vertical wind observations with two Fabry-Perot interferometers at Poker Flat, Alaska, *J. Geophys. Res.*, *106*, 10,537–10,551.

Ishii, M., M. Kubota, M. Conde, R. W. Smith, and M. Krynicki (2004), Vertical wind distribution in the polar thermosphere during Horizontal *E* Region Experiment (HEX) campaign, *J. Geophys. Res.*, *109*, A12311, doi:10.1029/2004JA010657.

Johnson, F. S., W. B. Hanson, R. R. Hodges, W. R. Coley, G. R. Carignan, and N. W. Spencer (1995), Gravity waves near 300 km over the polar caps, *J. Geophys. Res.*, *100*(A12), 23,993–24,002.

Knipp, D., S. Eriksson, L. Kilcommons, G. Crowley, J. Lei, M. Hairston, and K. Drake (2011), Extreme Poynting flux in the dayside thermosphere: Examples and statistics, *Geophys. Res. Lett.*, *38*, L16102, doi:10.1029/2011GL048302.

Kosch, M. J., M. Ishii, A. Kohsiek, D. Rees, K. Schlegel, T. Hagfors, and K. Cierpka (2000), A comparison of vertical thermospheric winds from Fabry-Perot interferometer measurements over a 50 km baseline, *Adv. Space Res.*, *26*(6), 985–988.

Oyama, S., B. J. Watkins, S. Maeda, H. Shinagawa, S. Nozawa, Y. Ogawa, A. Brekke, C. Lathuillere, and W. Kofman (2008), Generation of the lower-thermospheric vertical wind estimated with the EISCAT KST radar at high latitudes during periods of moderate geomagnetic disturbance, *Ann. Geophys.*, *26*, 1491–1505.

Price, G. D., R. W. Smith, and G. Hernandez (1995), Simultaneous measurements of large vertical winds in the upper and lower thermosphere, *J. Atmos. Terr. Phys.*, *57*(6), 631–643.

Rees, D., M. F. Smith, and R. Gordon (1984), The generation of vertical thermospheric winds and gravity waves at auroral latitudes–II. Theory and numerical modelling of vertical winds, *Planet. Space Sci.*, *32*(6), 685–705.

Richmond, A. D. (2010), On the ionospheric application of Poynting's theorem, *J. Geophys. Res.*, *115*, A10311, doi:10.1029/2010JA015768.

Ridley, A. J., Y. Deng, and G. Tóth (2006), The global ionosphere-thermosphere model, *J. Atmos. Sol. Terr. Phys.*, *68*, 839–864.

Shinagawa, H., and S. Oyama (2006), A two-dimensional simulation of thermospheric vertical winds in the vicinity of an auroral arc, *Earth Planets Space*, *58*, 1173–1181.

Shinagawa, H., S. Oyama, S. Nozawa, S. C. Buchert, R. Fujii, and M. Ishii (2003), Thermospheric and ionospheric dynamics in the auroral region, *Adv. Space Res.*, *31*(4), 951–956, doi:10.1016/S0273-1177(02)00792-5.

Sica, R. J., G. Hernandez, G. J. Romick, M. H. Rees, and R. G. Roble (1986), Auroral zone thermospheric dynamics: 2. Individual nights, *J. Geophys. Res.*, *91*(A12), 13,593–13,611.

Sipler, D. P., M. A. Biondi, and M. E. Zipf (1995), Vertical winds in the midlatitude thermosphere from Fabry-Perot Interferometer measurements, *J. Atmos. Terr. Phys.*, *57*(6), 621–629.

Smith, R. W. (1998), Vertical winds: a tutorial, *J. Atmos. Sol. Terr. Phys.*, *60*, 1425–1434.

Smith, R. W. (2000), The global-scale effect of small-scale thermospheric disturbances, *J. Atmos. Sol. Terr. Phys.*, *62*, 1623–1628.

Smith, R. W., and G. Hernandez (1995), Vertical winds in the thermosphere within the polar cap, *J. Atmos. Terr. Phys.*, *57*(6), 611–620.

Spencer, N. W., L. E. Wharton, G. R. Carignan, and J. C. Maurer (1982), Thermosphere zonal winds, vertical motions and temperature as measured from Dynamics Explorer, *Geophys. Res. Lett.*, *9*(9), 953–956.

Sun, Z.-P., R. P. Turco, R. L. Walterscheid, S. V. Venkateswaran, and P. W. Jones (1995), Thermospheric response to morningside diffuse

aurora: High-resolution three-dimensional simulations, *J. Geophys. Res.*, *100*(A12), 23,779–23,793.

Thayer, J. P., and J. Semeter (2004), The convergence of magnetospheric energy flux in the polar atmosphere, *J. Atmos. Sol. Terr. Phys.*, *66*(10), 807–824.

Walterscheid, R. L., and L. R. Lyons (1992), The neutral circulation in the vicinity of a stable auroral arc, *J. Geophys. Res.*, *97*(A12), 19,489–19,499.

Walterscheid, R. L., L. R. Lyons, and K. E. Taylor (1985), The perturbed neutral circulation in the vicinity of a symmetric stable auroral arc, *J. Geophys. Res.*, *90*(A12), 12235–12248.

Wardill, P., and F. Jacka (1986), Vertical motions in the thermosphere over Mawson, Antarctica, *J. Atmos. Terr. Phys.*, *48*(3), 289–292.

Yiğit, E., and A. J. Ridley (2011), Role of variability in determining the vertical wind speeds and structure, *J. Geophys. Res.*, *116*, A12305, doi:10.1029/2011JA016714.

C. Anderson and M. Conde, Geophysical Institute, University of Alaska Fairbanks, Fairbanks, AK 99775, USA. (callum@gi.alaska.edu)

M. G. McHarg, Physics Department, U.S. Air Force Academy, 2354 Fairchild Hall, Ste. 2A31, Colorado Springs, CO 80840, USA.